Drag Force as a Tool to Test the Active Mechanical Response of PC12 Neurites

Roberto Bernal,[†*] Francisco Melo,[†] and Pramod A. Pullarkat[‡]
[†]Departmento de Física and Center for Advanced Interdisciplinary Research in Materials, Universidad de Santiago de Chile, Santiago, Chile; and [‡]Raman Research Institute, Sadashivanagar, Bangalore, India

ABSTRACT We investigate the mechanical response of PC12 neurites subjected to a drag force imposed by a laminar flow perpendicular to the neurite axis. The curvature of the catenary shape acquired by an initially straight neurite under the action of the drag force provides information on both elongation and tension of the neurite. This method allows us to measure the rest tension and viscoelastic parameters of PC12 neurites and active behavior of neurites. Measurement of oscillations in the strain rate of neurites at constant flow rate provides insight on the response of molecular motors and additional support for the presence of a negative strain-rate sensitivity region in the global mechanical response of PC12 neurites.

INTRODUCTION

For decades, a variety of experimental methods has provided valuable information to enable us to understand cell mechanical behavior at the subcellular scale. Such techniques include thin elastic substrates (1,2), micropattern-coated substrates (3,4), microneedles and microplates (5–8), magnetic (9) and optical (10,11) tweezers, and atomic force microscopy (12).

Given the complexity involved in fully describing the mechanical properties of cells (in which three-dimensional network of filaments and molecular motors interact in a complex way), increasing effort is being given to elucidating the mechanics of quasi-one-dimensional cells. These cells, although nearly one-dimensional from the geometric and mechanical point of view, have all the components of regular cells—for instance, they contain cytoplasm, actin networks, microtubules, intermediate filaments, motor proteins, and ion channels.

PC12 neurites show interesting mechanical response under external mechanical load, including viscoelastic elongation and active contraction due to the action of molecular motors and their interaction with microtubules and the actin network. It is important to notice that even in the absence of external forces, due to their active component, neurites are found at a residual tension (6). As demonstrated in the literature (5,6,8), it is a good simplifying assumption to model PC12 neurites as linear springs. The simple geometry of these cells facilitates a description of the interaction of cells and its environment. In fact, a neurite can be approximated as a combined mechanical device that includes linear springs, a linear dashpot (5,6), and a nonlinear device (8) accounting for the active response. To validate such a simplified model, it is necessary to investigate how physiological variables such adenosine-triphosphate concentration, molecular motor type and spatial configuration (randomly oriented versus muscle fiber type), microtubule arrangement and actin network dynamics affect the main features of these mechanical devices. A recent study suggests (8) that certain neurites combine those parameters such that the resulting tension response exhibits negative strain-rate sensitivity. This would explain the abrupt time transition between viscous relaxation and active contraction of neurites that was observed experimentally. On the other hand, new and sensitive techniques are required to better assess the dynamical responses of biological structures undergoing investigation. With this goal in mind, we describe here a fluid-mechanics-based technique suitable for impose a drag force acting perpendicular to a PC12 neurite axis. Drag force has the advantage of being homogeneously distributed along the neurite. The curvature of the catenary shape acquired by an initially straight neurite under the action of the drag force provides us with valuable information on both elongation and tension along the neurite, allowing us to investigate the viscoelastic and active response of neurites. Dynamical response of neurites under sudden changes on drag force is also investigated and relevant information about the initial neurite tension and its main elastic constant is obtained using this procedure. The analysis of the neurite elongation over time provides useful information to estimate the neurite internal tension and the secondary elastic constant. In turn, the examination of spontaneous and nearly periodic contraction-elongation cycles of the neurites observed at constant flow provides insight on the nonlinear response of molecular motors (8).

Neurite equilibrium under drag forces

Microneedle methods have proved valuable for testing the mechanical response of neurites (5,6,8). Specifically, these methods allow us to measure the main elastic constant κ, the secondary elastic constant k, the internal friction γ, and the initial tension T_o of a neurite (Fig. 1 *a*). The global

Submitted April 8, 2009, and accepted for publication October 7, 2009.

*Correspondence: roberto.bernal@usach.cl

Editor: Denis Wirtz.

0006-3495/10/02/0515/9 $2.00

doi: 10.1016/j.bpj.2009.10.024

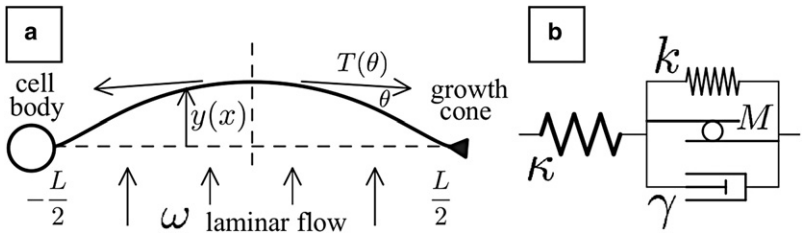

FIGURE 1 (*a*) Schematic view of a neurite under a viscous force ω. (*b*) Mechanical representation of a neurite; the interaction between the filaments and molecular motors are represented by the elements κ, k, γ, and M, where M represents molecular motors response (8).

response of molecular motors, represented by a Gaussian function with a typical force scale given by T_a and a typical velocity for nonloaded motors v, has been assessed with this method as well (8). However, a mechanical test using microneedles becomes less suitable to explore these properties in weak neurites. For weak neurites, the initial tension T_o (deduced under a mechanical test) might become negligible, in comparison with the elastic tension. In addition, weak neurites, for instance those previously treated with specific drugs, are much more sensitive to damage at the microneedle contact. Our method consists in applying well-controlled distributed forces on neurite by using a laminar flow perpendicular to the neurite longitudinal axis. Thus, a neurite can be represented as a string with fixed ends at $x = \pm L/2$ under the influence of a force field ω that depends on the neurite radius, the velocity of the fluid, and the fluid viscosity (Fig. 1 *a*). The drag force is balanced by the mechanical tension at each point of the neurite that reaches a catenary shape with nearly constant tension (see Appendix for details).

On the other hand, as described in Bernal et al. (8), neurites under an external force are modeled mechanically as a combination of classical mechanical devices and the response of molecular motors (Fig. 1 *b*), where its components experience elongation δ_κ for the elastic component κ and δ_k for the elements k-γ-M. Then, the mechanical equilibrium is described by

$$\kappa\delta_\kappa + T_o = T(\delta l), \tag{1}$$

$$k\delta_k + \gamma\dot{\delta}_k + T_a e^{-\dot{\delta}_k^2/v^2} = T(\delta l), \tag{2}$$

$$\delta_\kappa + \delta_k = \delta l, \tag{3}$$

where T_o is the initial state of tension of the neurite, $M = T_a e^{-\dot{\delta l}^2/v^2}$ is the molecular motors mechanical response, T_a is the maximum tension of molecular motors and v their characteristic average speed, δl is the total elongation, and $T(\delta l)$ is the tension of the neurite. Describing the elongations δ_κ and δ_k as a function of δl of the previous set of equations leads to

$$\left(1 + \frac{k}{\kappa}\right)T(\delta l) + \frac{\gamma}{\kappa}\dot{T}(\delta l) = k\delta l + \gamma\dot{\delta l} + T_a e^{-\left(\dot{\delta l} - \frac{1}{\kappa}\dot{T}(\delta l)\right)^2/v^2} + \frac{k}{\kappa}T_o, \tag{4}$$

which represents the mechanical equilibrium of the neurite under the drag imposed by the laminar flow in terms of its total elongation δl. Below we describe simple experimental procedures that allow the assessment of the main mechanical parameters of neurites included in Tan et al. (4).

See Table 1 for nomenclature used in this article, and Table 2 for values reported by us compared to those reported in the literature (5,8).

METHODS

Cells culture and experimental setup

Nerve growth factor-7S (NGF), nocodazole (noco), amino-silane, and rat tail collagen were obtained from Sigma-Aldrich Chemical (St. Louis, MO), and latrunculin-A (lat-A) was obtained from Molecular Probes (Eugene, OR). Cover glasses ($\phi = 20$ mm) were previously immersed for 1 h into a 90% ethanol, 8% H_2O, and 2% aminosilane solution, then rinsed with ethanol and dried at room temperature. Glass cylinders (Fig. 2 *a*) with dimensions 10-mm diameter and 10-mm high and 2-mm wall thickness were placed over the cover glasses and exposed to ultraviolet light for 15 min. After that, 200 μL solution of 1% diluted collagen and 90% ethanol was added and allowed to dry. The culture of cellular line PC12 was made over five days using RPMI 1640 medium (GIBCO, Billings, MT) with 10% horse

TABLE 1 Nomenclature

κ	Main spring constant
k	Secondary spring constant
γ	Neurite dissipation
T_a	Maximum tension applied by the molecular motors
T_o	Neurite initial tension
v	Molecular motor speed
M	Molecular motors mechanical response
Γ	Nondimensional dissipation ratio
δ_κ	Elongation of the element κ
δl	Neurite total elongation
δ_k	Elongation of the elements k-γ-M
τ, Θ	Timescales
L	Neurite initial length
T	Neurite tension
C	Neurite curvature
r	Neurite radii
μ	Neurite internal viscosity
ρ_l	Neurite linear density
U	Fluid velocity
ρ	Fluid density
ν	Fluid kinematic viscosity
η	Fluid dynamic viscosity
R	Needle radii
L	Needle length
Δ	Needle tip deflection
ω	Drag force

TABLE 2 Comparison of values reported in the literature (5,8) and in this article

Model	Dennerll et al. (5)	Bernal et al. (8)	This article
κ (mN/m)	0.1–0.7	0.05–0.6	0.4–0.5
k (mN/m)	~6×10^{-3}	10^{-3}–10^{-2}	10^{-3}–10^{-1}
γ (mN·s/m)	~6	0.5–2	4–10
T_o (nN)	···	0–2	0–1.2
T_a (nN)	···	0–1.5	0–1.2
v (μm/s)	···	0.01–1	0.01–1
μ (Pa·s)	···	···	10^4–10^5

serum and 5% fetal calf serum and 50 ng/mL of NGF (this medium was changed every two days). The glass cylinder was then removed and the cover glass with the PC12 cells was placed in the flow chamber (Fig. 2 *b*). For experiments we used normal culture medium, or RPMI 1640 medium (GIBCO) with 25-mM HEPES and L-glutamine with serum. Flow experiments were performed in a stainless steel chamber with an internal volume $10 \times 5 \times 1(\text{mm})^3$. This chamber is introduced into a second aluminum chamber maintained at constant temperature of 36.8 ± 0.2°C using a thermal bath (DC1; Haake, Thermo Electron, Newington, NH), and monitored by a platinum resistance sensor (Pt100). Observations were made using an Axiovert-135 microscope (Carl Zeiss, Oberkochen, Germany) in phase contrast mode. Images were acquired using a Spot-RT charge-coupled device camera (Diagnostic Instruments, Sterling Heights, MI) and MetaVue 6.1 software (Molecular Devices, Dowington, PA), with a final magnification of 0.2 μm/pixel. Experiments using altered medium without serum or noco (10 μg/mL) (13) or lat-A (0.2 μg/mL) (14), were switched using a three-way valve.

Flow velocimetry and drag force calibration

In experiments, flow was driven by a syringe controlled by a DC motor at flow rates up to 30 μL/s. The flow rate at given flow conditions was measured by adding latex beads, 0.5 μm in diameter, into the fluid chamber, and by tracking these particles, which are at the same plane of the neurite. The obtained flow field did not show variations or periodic fluctuations at the explored range of injected fluxes.

Theoretically, the drag force acting on an infinitely long cylinder, oriented perpendicular to the flow, is given by $\omega = 4\pi\eta U/\ln(3.7\nu/rU)$ (15), where η and $\nu = \eta/\rho$ are the dynamic and kinematic viscosities, respectively; ρ is the density of the fluid (culture medium GIBCO at 37°C; $\rho = 1.0745$ g/cm^3; $\eta = 8.9 \times 10^{-4}$ Pa·s); and r is the mean radius of the neurite surrounded by a fluid at the velocity U.

To check the applicability of the above formula in our case, we performed independent measurements of the drag force by using a calibrated microneedle ($R = 16$ μm) intended to mimic a typical neurite. In our technique, a calibrated microneedle placed perpendicular to the flow in a plane parallel and close to the coverslip surface (50 μm above the surface) undergoes a load per unit length given by $dF/dx = -\omega$ or $F(x) = \omega(x - \mathcal{L})$, where ω is the drag force and $\mathcal{L}$ the length of the needle (16). The deflection profile of the needle is given by the differential equation $EId^3y(x)/dx^3 = F(x)$, where E is the Young's modulus of glass and I is the moment of the needle. Solving for the deflection profile $y(x)$ and evaluating the solution at $x = \mathcal{L}$, we obtain the maximum deflection of the needle tip Δ, and the load per unit of length, $\omega = (8EI/\mathcal{L}^4)\Delta$. The fluid speed at the same plane of the needle is found using the same procedure described above. Our measurements of ω by means of the needle deflection and our independent measurement of fluid velocity show that ω is given in a good approximation by the drag formula (Fig. 2, *c* and *d*).

Tension and elongation measurements

For a constant value of the drag force ω, tension along the neurite can be inferred from an analysis of its curved shape obtained from experimental snapshots (Fig. 3), by fitting it to the profile given by Eq. 11. In practice, from such fit we measure the curvature at the middle point of the catenary, $y''_{x=0} \approx C$, and we then obtain the neurite tension as $T = \omega/C$. To check the validity of our method, curvature is calculated directly from image analysis by extracting the middle line along the neurite (*dashed lines* on images) and by calculating the derivative of such data (averaged over a distance equal to a neurite radius; Fig. 3, *middle panel*).

In some cases, as the one presented in Fig. 3 (*top panel*), the neurite is slightly inclined with respect to the glass plate and neurites appear out of focus near the cell body. Because the flow speed increases with distance from the substrate, higher values of curvature are expected in this region. However, as seen in the lower panel of the Fig. 3, the curvature presents variations only in a region that is very close to the cell body and does not affect significantly our estimate of average curvature.

On the other hand, given the relatively small elongations, the curvature C can be used to link the neurite elongation to the neurite tension. This is done by writing the total neurite length, under the viscous flow, as the line integral of Eq. 11 minus the initial length, which produces $\delta l \simeq C^2L^3/24$. Then, the neurite tension as a function of its elongation δl reads

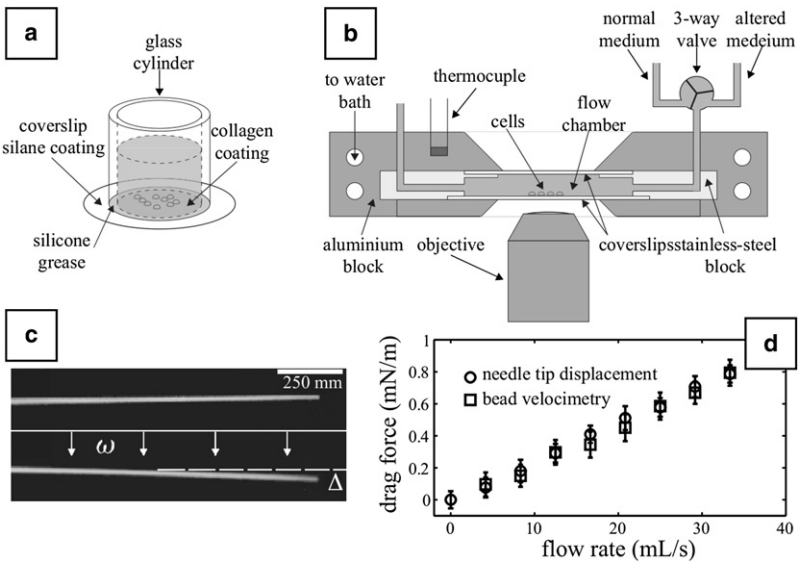

FIGURE 2 (*a*) PC12 neurites are grown inside glass wells placed on collagen-coated coverslips and the coverslips and later transferred to the flow chamber. (*b*) Schematic of the flow-chamber setup. The three-way valve is used for fast switching between normal medium and medium containing specific drugs without affecting the steady-state flow rate (pump is always on). (*c*) Needle under the effect of viscous drag ($L = 3$ mm, $R = 16$ μm). (*d*) Comparison of the measured drag force using the needle technique and beads velocimetry.

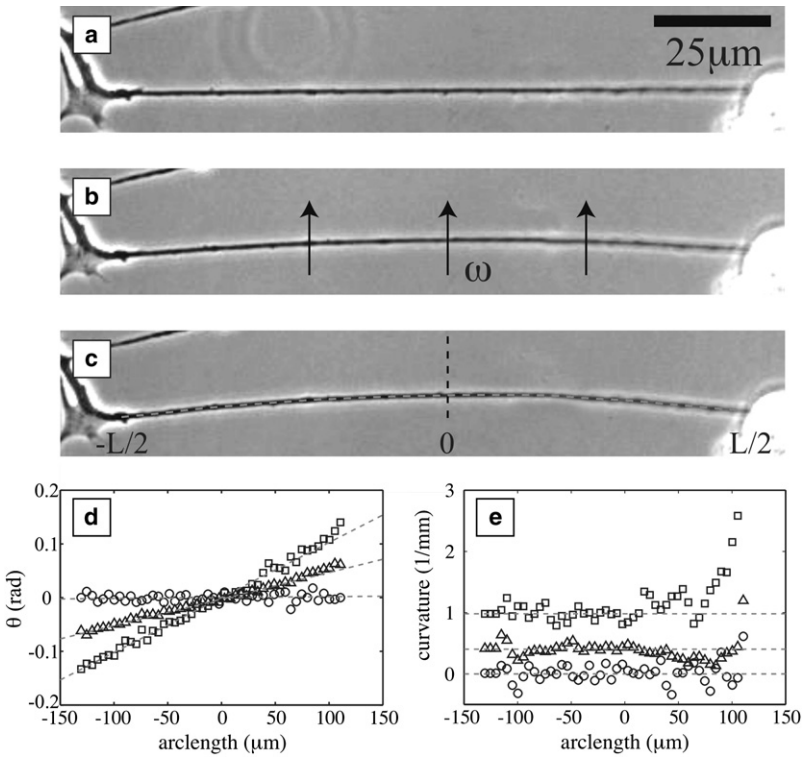

FIGURE 3 (*a*) Initial straight PC12 neurite without flow. (*b* and *c*) Effect of the drag force 30 and 60 s after the flow is turned on, respectively. (*c*, *dashed line*) Middle axis of the neurite obtained by image analysis. (*d*) The angle θ between the neurite axis and the horizontal for the three cases depicted in panels *a*, *b*, and *c*, respectively. (*e*) The calculated curvature obtained from data presented in panel *d*.

$$T(\delta l) \simeq \sqrt{\frac{L^3\omega^2}{24\delta l}}, \tag{5}$$

which closes the mechanical equilibrium equations expressed by Tan et al. (4).

RESULTS

Experiments performed using the laminar flow technique were set to test and measure each parameter of our model, which is represented by Eq. 4. In this article, the radii r values of neurites under investigation are in the 0.6–1.0-μm range, whereas its lengths L range between 100 and 200 μm. Only those neurites which are found nearly perpendicular to the flow axis were used. For a given drag force ω, tension over time at the middle point of the neurite is obtained from a fit of the experimental neurite profile by using $T = \omega/C$. Note that typical values are $T = 0.1$ nN and $\omega = 10$ nN/m, for the neurite tension and drag force, respectively. Introducing these representative values later into Eq. 12 produces $\cosh(\omega L/2T) \approx 1$, which confirms that tension along the neurite can be considered constant.

Elastic constant and initial neurite tension

The main elastic constant κ and the initial neurite tension T_o are measured by increasing the drag force in steps. Each flow value is maintained during 400 s and then it is increased by equal steps, as shown in Fig. 4 *a*. The imposed flow velocity ranged between 10 and 100 μm/s. The analysis shows sudden elongation events immediately after each flow step whereas neurite tension seems to remain roughly constant (Fig. 4 *a*). For the data analysis, we use the simplified neurite model presented in the literature (5,8) and sketched in Fig. 1 *b*. Given the small value of the secondary elastic constant k compared to κ and the presence of a dashpot in

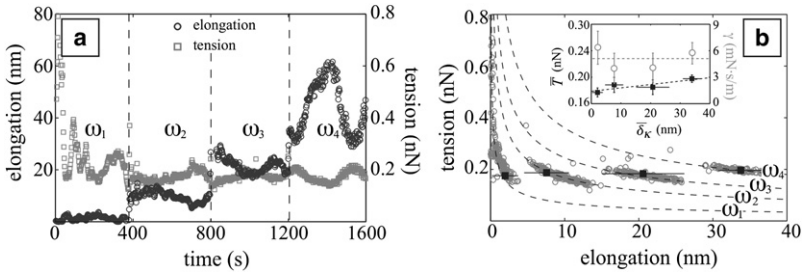

FIGURE 4 (*a*) Drag-step experiment: $\omega_1 = 14.7$, $\omega_2 = 29.4$, $\omega_3 = 42.2$, and $\omega_4 = 63.3$ nN/m on an initial PC12 neurite length $L \approx 198$ μm shows correlated elongations at these drag increments with an average tension $\langle T \rangle \approx 0.18 \pm 0.08$ nN throughout the course of the experiment under normal serum conditions. (*b*) Tension versus elongation data for the ω values. (*Inset*) Average tension $\overline{T}$ and elongation $\overline{\delta}_\kappa$ values after the drag-step increment; the intersection value corresponds to the initial neurite tension $T_o = 0.18 \pm 0.02$ nN and the slope to the main spring restitution constant $\kappa = 0.51 \pm 0.14$ mN/m. Neurite dissipation is also plotted at each drag step with an average value of $\gamma = 4.9 \pm 1.3$ mN·s/m.

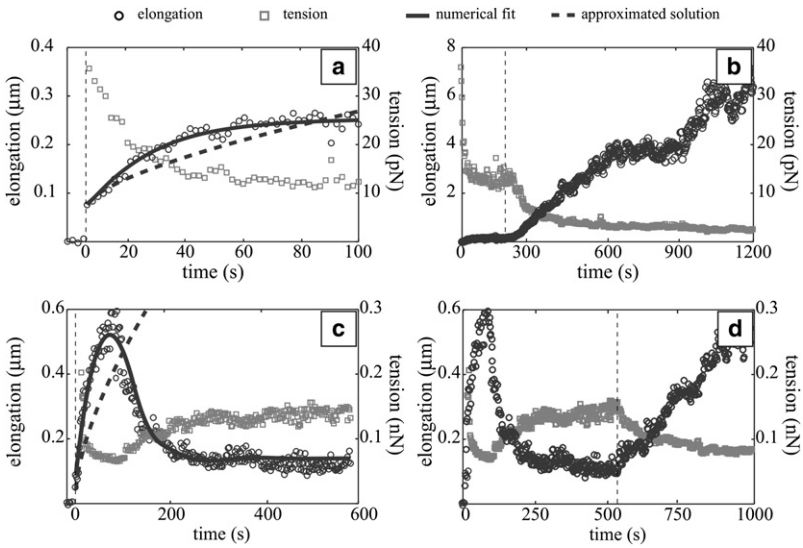

FIGURE 5 (*a*) Viscoelastic response for a PC12 neurite in medium with a normal concentration of serum. The applied drag force $\omega = 29.4$ nN/m, and initial neurite length $L = 95$ μm. (*b*) Effect of lat-A over the same neurite as in panel *a*. Lat-A was added after 150 s of observation under the same experimental conditions (indicated by a *dashed vertical line*). (*c*) PC12 neurite that shows active contraction after an initial viscoelastic elongation. The imposed drag force $\omega = 56.9$ nN/m with an initial neurite length $L = 245$ μm. (*d*) The effect of noco over the same neurite as in panel *c*. Noco was added after 600 s of observation under the same experimental conditions (indicated by a *dashed vertical line*). Solid lines in panels *a* and *c* represent the numerical solution for both cases. Dashed lines in panels *a* and *c* show the approximated solution (Eq. 16) using the parameter values obtained from the numerical fit, considering the data before the drug treatment.

parallel with k (5,8), only the main elastic response can compensate the fast increase in neurite elongation. Thus, from Eq. 1 and considering that most of the elongation during the step corresponds to the element κ, we obtain

$$\kappa\delta_\kappa + T_o = \sqrt{\frac{\omega^2 L^3}{24\delta_\kappa}}. \quad (6)$$

In Fig. 4 *b*, dashed lines represent the tension of neurite given by the flow conditions (right term of Eq. 6 as a function of δ_κ) obtained for each value of ω. At equilibrium, all data points are on one of these curves. It can be seen that neurite tension does not vary significantly with δ_κ. However, it is possible to obtain an estimate of κ by taking the slope of the total tension as the function of the average δ_κ. This is represented by the straight line in the inset of Fig. 4 *b*, where data were averaged in a 10 s window after each flow step.

Viscoelastic relaxation

In the workframe provided by our simple mechanical model, after the sudden elastic elongation, the elements k-M-γ must slowly elongate. To investigate such slow evolution, observations at larger timescales are performed at constant flow parameters. In Fig. 5, *a* and *c*, the fast elastic elongation resulting from the sudden flow increase is indeed followed by a slow viscoelastic relaxation which, in some cases, is also followed by a neurite active contraction due to the global response of protein motors (8) (Fig. 5 *c*). Notice that at sufficiently large timescale, the main contribution to the total elongation is the viscoelastic element with elongation δ_k. Then, it is possible to follow the dynamics of the elements k-M-γ by assuming $\delta_k \approx \delta l - \delta_\kappa^0$, as a simplifying assumption of Eq. 6. This is

$$k(\delta l - \delta_\kappa^0) + \gamma\dot{\delta l} + T_a e^{-\dot{\delta l}^2/v^2} \simeq T(\delta l), \quad (7)$$

where $\delta^0{}_\kappa$ corresponds to the sudden elastic elongation.

In both figures, the typical elongation rate is small compared to the typical velocity scale v of nonloaded motors. Then, to obtain a preliminary estimate of the internal friction γ, the response of the molecular motors $T_a e^{-\dot{\delta l}^2/v^2}$ can be approximated to T_a, and Eq. 7 can be reduced to (see Appendix)

$$\delta l(t) = \left(\left(\frac{3}{32}\right)^{1/2} - \frac{\mathcal{T}}{\omega L}\right)^{2/3} \left(\frac{\omega t}{\gamma}\right)^{2/3} L, \quad (8)$$

where the external force is balanced only by the internal friction of the neurite and its initial tension, with $T = T_a - k\delta^0{}_\kappa$. Notice that most of our experimental data shows ratios $T/\omega L < 0.3$.

With the help of Eq. 8, an approximated value for the neurite internal friction γ is obtained from a fit to the experimental data at early stages of elongation ($t < 10$ s). The value obtained is used for a more elaborate fit of experimental data by integrating numerically Eq. 7. This is done by using the initial experimental slope as an initial condition, the final tension at the steady state for T_a and the starting values of γ and k, from the approximate solution, as a trial of the true parameters. As shown in the inset of Fig. 4 *b*, we have measured the dissipation constant taking into account the neurite elongation at each drag step in a 10 s span window, obtaining a reasonable value of $\gamma = 4.9 \pm 1.3$ mN·s/m. Values for the parameters γ, k, T_a, and v are in the range of those obtained in the literature (5,8). The numerical integration of Eq. 7 reproduces both viscoelastic elongation and active contraction behaviors after fitting the model to the experimental data. As shown in Fig. 5, *a* and *c*, the numerical solutions (*solid lines*) and the approximate solution (Eq. 16) for early stages of elongation (*dashed lines*) using the values obtained from the numerical fit, are valid for timescales $t < 10$ s, as expected.

Effective viscosity of neurites

On the other hand, as demonstrated in the literature (8,17) it is possible to relate the neurite dissipation to the interaction

of the molecular motors with the inner biopolymers in the neurite structure. The case of a purely viscous bridge under the effect of gravity, studied by Teichman and Mahadevan (18), allows us to relate the internal viscosity of PC12 neurite to the dissipation constant γ, as we show in the following. In fact, by using Eq. 16 and the approximated parabolic solution to the catenary shape, it can be easily shown that the maximum height of the curved neurite is $H_{\text{neurite}} \simeq 6^{2/3}/8(\omega/\gamma)^{1/3}Lt^{1/3}$. In turn, the solution obtained by Teichman and Mahadevan for a purely viscous bridge under the action of gravity predicts that $H_{\text{bridge}} \simeq (12w/\mu AL^2)^{1/3}L^2t^{1/3}$, with A as the cross-sectional area of the viscous bridge, L its initial length, and w the respective gravitational force per unit of length, which has the same role as the drag force ω. The viscous-bridge solution is valid when changes in the cross-sectional area of the viscous fluid can be neglected for a timescale given by $t_c \sim \mu h^5/wL^4$ (h initial diameter). Comparing H_{neurite} to H_{bridge}, we obtain $\mu = 512L\gamma/3A$, giving us an average value for the neurite viscosity μ that is within the range of 10^4–10^5 Pa·s, and which is 10–100 times larger than the average viscosity of living cells (19,20). This difference in the viscosity values could be a consequence of the dissimilarity at the subcellular organization of the cytoskeleton between cells (randomly oriented) and neurites (axially oriented).

Drug effects on mechanical properties of neurites

To show the suitability of the flow method to assess the mechanical features of PC12 due to changes in environmental conditions, in the following we show the typical mechanical response of neurites induced by the effect of two well-known drugs that can be mixed with the testing fluid. In the first example we explore the effect of the depolymerization of specific subcelular structures, such as the actin network, by using lat-A. In the second example, we test the effect of noco, a drug known for inducing a depolymerization on the microtubules network. Neurite responses for both cases are shown in Fig. 5, parts *b* and *d*, respectively.

In Fig. 5 *b*, after the equilibrium is reached, the tension of neurite is nearly 10 pN. The medium containing the lat-A drug is then injected into the fluid without changing the flow conditions (*vertical dashed line*). We used a concentration 0.2 μg/mL. Above such value, it has been shown in Spector et al. (14) that actin depolymerization rate no longer depends on lat-A concentration. An abrupt decrease of tension, accompanying a monotonous increase of neurite elongation, is observed immediately after drug injection Fig. 5 *b*. The elongation rate induced by lat-A drug is ~0.01 μm/s, with a neurite tension that almost vanishes after a 1200 s.

In Fig. 5 *d*, noco injection, in a concentration of 10 μg/mL (13), occurs at 550 s (*dashed line*). Immediately after, neurites exhibit a continuous elongation. The elongation rate induced by noco is ~0.001 μm/s, a value significantly smaller than that of lat-A for the same test. The rest-tension of neurite directly after noco injection is ~150 pN, decreasing by a factor of two (~90 pN) after the noco effect.

In terms of the PC12 neurite mechanical representation, lat-A and noco act selectively on each mechanical device. Using lat-A, we observed a continuous elongation of the neurite with a monotonous degression of tension. In other words, the elastic components were gradually affected by the depolymerization of the actin network and only the dissipation device seems to remain. Note that the timescale of force relaxation is consistent with the time for which a complete depolymerization network is expected (13). On the other hand, using noco, we observed an exponential relaxation to a different state of equilibrium of a smaller but significant tension. Thus, we believe that the depolymerization of microtubules by noco modifies the internal friction of the neurite—leaving, after its effect, a tubulin monomer solution surrounded by an intact actin network. Given the high value of the final tension after microtubules depolymerization, this result would seem to suggest that both the elastic and the active response of neurite are mainly due to the actin network and molecular motor therein. However, Dennerll et al. (21) observed an increase in the neurite rest-tension (their Fig. 9) after 10–15 min of noco injection—which seemed to indicate the actin network was mainly responsible for the actions of PC 12 cells. From these results, it is clear that investigation of the active response after a complete depolymerization of the actin network and/or microtubules, will require additional experimental effort to gain detailed understanding of drug effect on PC12 neurites.

DISCUSSION

The response of PC12 neurites shows viscoelastic relaxation and active contraction (Fig. 5) as previously reported in Bernal et al. (8). This behavior has been captured by modeling the global action of molecular motors using an effective Gaussian response of maximum force T_a and a typical velocity v at which molecular motor becomes ineffective. This model implies that, for specific combinations of the model parameters, a region of negative sensitivity exists in the tension-strain rate curve. Consequently, neurites might exhibit relaxation oscillations characteristic of nonlinear systems. As demonstrated in Fig. 6, such oscillations take place in normal conditions of cell medium at a constant flow rate. However, the applied drag force, for this particular case, is comparable to the maximum tension of the global molecular motors response, T_a.

To study the general features of the relaxation oscillations shown in Fig. 6, Eq. 7 is now written in terms of the variables tension and elongation rate only, which defines the characteristic response curve of a neurite:

$$T(\dot{\delta}l) - k\frac{\omega^2 L^3}{24\,T(\dot{\delta}l)^2} = \gamma\dot{\delta}l + T_a e^{-\dot{\delta}l^2/v^2}.$$

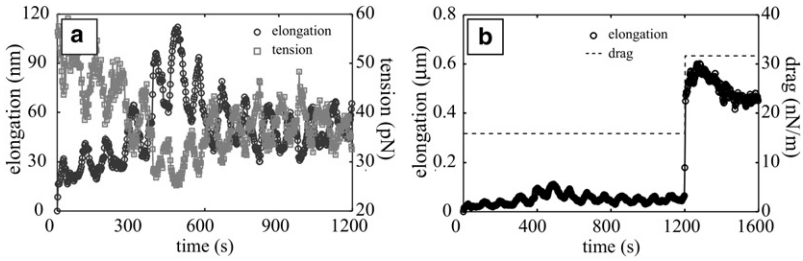

FIGURE 6 (*a*) Oscillations in PC12 length at constant drag force $\omega = 15.8$ nN/m and an initial length $L = 196\ \mu$m. These oscillations are the result of a periodic transition from a viscoelastic relaxation to an active contraction with a timescale $\tau \approx 100$ s. (*b*) After 20 min, the oscillatory behavior change by increasing the drag force in a factor two, $\omega = 31.6$ nN/m, and the timescale of the cycle increases by a factor 4, $\tau \sim 400$ s. See Appendix for an estimate of timescale of relaxation oscillations.

This contains a fixed point or attractor (Fig. 7 *a*), which represents a stable mechanical state at null rate of elongation and tension T_a. The existence of inflection points in the curve is given by the relation

$$\Gamma = \frac{\dot{\delta l}}{v} e^{-\dot{\delta l}^2/v^2},$$

where $\Gamma \equiv \gamma v/2T_a$, whose maximum value is $\Gamma_c = 1/\sqrt{2e} \approx 0.4289$ (Fig. 7 *b*). Thus, when $\Gamma < \Gamma_c$, two points exist at which $\partial T/\partial \dot{\delta l} = 0$. When $\Gamma \geq \Gamma_c$, the response curve is monotonous, indicating that only monotonous relaxation can take place (Fig. 5 *a*). However, trajectories of viscoelastic relaxation followed by active contraction occur for values $\Gamma < \Gamma_c$ (Fig. 7 *b* and Fig. 5 *c*). Both situations are depicted in Fig. 7 *c*, demonstrating that when the initial tension T is larger than T_a, for a set of values of the parameters γ, T_a, and v, a neurite will show either pure viscoelastic relaxation or an active response with trajectories attracted to the stable point $\dot{\delta l} = 0$ at the T-$\dot{\delta l}$ plane.

In this framework, the experimental neurite oscillations presented in Fig. 6 are then schematized in Fig. 7 *d*; and these would then correspond to a case in which the linear stable point at $\dot{\delta l} = 0$ becomes sensitive enough to experimental fluctuations to sustain consecutive relaxation cycles. Similar spontaneous oscillatory contraction has been reported in actin filaments (22) and shape oscillations of fibroblast as a result of loss of cell-substrate adhesion with a timescale of ~50 s (23). Oscillatory behavior of collective molecular motors has been also modeled in Jülicher and Prost (24).

In conclusion, the drag force method can be used to measure: small forces exerted on neurites that have been treated with a low concentration of serum to reduce the activity of molecular motors; disruption of the actin network and/or microtubules upon the addition of a drug; and outcomes from knocking out specific molecular motors. In other words, it is a suitable tool for measuring variables that play essential roles in intracellular transport, cell shape, and motility. However, it can also be used to test simplified biological models. For example, it can be applied to nanometric tubular structures (which are fabricated, by pulling, from giant unilamellar vesicles (25)), and used in exploring their response, as functions of a controlled composition of subcellular structure into the vesicle, to the creation of more complex tubular membranes (26).

APPENDIX

Mechanical considerations

The mechanical equilibrium of neurite (Fig. 1 *a*) is given by

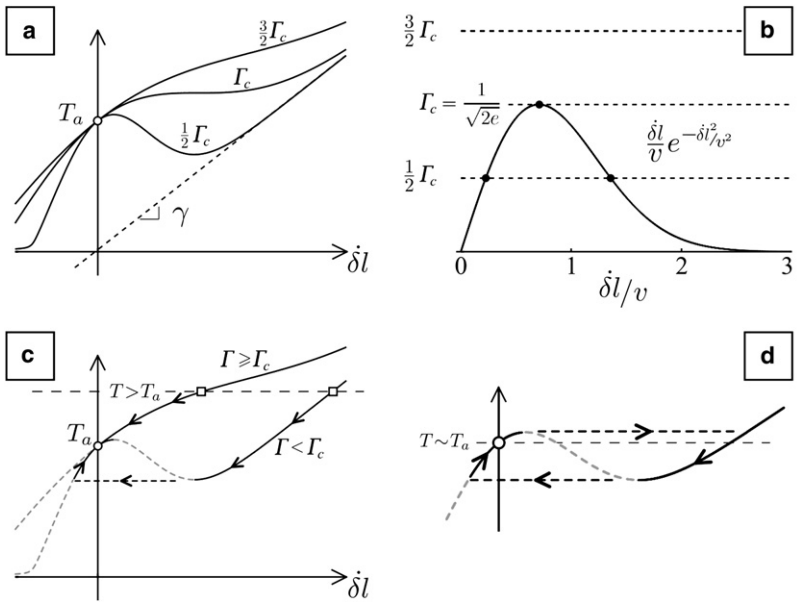

FIGURE 7 (*a*) Mechanical responses for three values of the dimensionless parameter Γ with fixed values for γ and T_a. (*b*) Conditional intersection to obtain active response. (*c*) Relaxation and active responses (□, starting points; ○, attractor) as a function of the dimensionless parameter Γ. (*d*) Schematic representation of the oscillatory response.

$$d(T(\theta)\cos(\theta)) = 0, \quad (9)$$

$$d(T(\theta)\sin(\theta)) = \omega ds. \quad (10)$$

The equilibrium condition in Eq. 9 gives the tension as a function of the angular coordinate θ as $T(\theta) = T/\cos(\theta)$, where T is the tension at the middle point ($\theta = 0$) (see Fig. 1 *a*). Inserting this result into Eq. 10 leads to

$$d(T\tan(\theta)) = \omega ds$$

or

$$d(Tdy/dx) = \omega\sqrt{1 + (dy/dx)^2}dx,$$

where x and y are the horizontal and vertical coordinates, respectively. The neurite shape, with fixed ends at $x = \pm L/2$, is then described by a catenary curve $y(x)$ and with tension $T(x)$, as

$$y(x) = \frac{T}{\omega}\cosh\left(\frac{\omega}{T}x\right) - \frac{T}{\omega}\cosh\left(\frac{\omega L}{2T}\right), \quad (11)$$

$$T(x) = T\cosh\left(\frac{\omega}{T}x\right). \quad (12)$$

The catenary given by Eq. 11 can be approximated by a parabolic function if $ds \approx dx$, i.e., if $\omega L/2T \ll 1$. Note that if $dy/dx << 1$, then $dT/dx \approx 0$ and $Td^2y/dx^2 \approx \omega$, and Eq. 11 becomes $y(x) \simeq (L^2 - 4x^2)\omega/8T$.

Inertial effects

To obtain some insight about the timescales involved, let us consider how the neurite relaxes its shape to a catenary when subjected to changes on the drag force. The dynamic equation, in the limit $dx \approx ds$, can be written as

$$\rho_l\frac{\partial^2 y}{\partial t^2} = T\frac{\partial^2 y}{\partial x^2} + \omega\left(1 - \frac{1}{U}\frac{\partial y}{\partial t}\right),$$

where ρ_l is the mass per unit of length, and ω is the viscous force that depends now on the relative velocity at the point $y(x, t)$, with a stationary solution $y_0(x) = (L^2 - 4x^2)\omega/8T$. Under a perturbation on flow, the new solution is, $y = y_0 + \delta y$, leading to

$$\rho_l\frac{\partial^2\delta y}{\partial t^2} + \frac{\omega}{U}\frac{\partial\delta y}{\partial t} = T\frac{\partial^2\delta y}{\partial x^2}.$$

Comparing the inertial and dissipation terms,

$$\rho_l\frac{\delta y}{\tau^2} \sim \frac{\omega}{U}\frac{\delta y}{\tau},$$

we obtain a timescale given by $\tau \sim \rho_l U/\omega$. Taking the density of cells as $\rho = 1$ g/cm^3, the average radius of a neurite as $r = 1$ μm, the velocity of the fluid near to the wall as $U \sim 100$ μm/s and the viscous drag associated with the flow as $\omega = 0.1$ μN/m, we obtain $\tau \sim 1$ μs. Thus, any transient due to neurite inertia can be neglected for timescales larger than τ.

Neurite radii effects

In general, local variations in curvature should be a result of changes either in flow velocity or neurite diameter. Particle tracking shows that relative fluctuations in fluid speed were <10%, affecting globally the curvature value ($C = \omega(U)/T$)). However, variations in the neurite radius are local, so we can model these by introducing the inhomogeneity into the calculation of the drag force at constant fluid velocity U, writing $r = r_o + \delta r$, the drag force per unit of length, $\omega = 4\pi\eta U/\ln(3.7\nu/rU)$, so that the relative variation of drag is $\delta\omega/\omega_o \approx (\omega_o/\omega_a)(\delta r/r_o)$, where $\omega_o = 4\pi\eta U/\ln(3.7\nu/r_o U)$ and $\omega_a = 4\pi\eta U$. Using our experimental values and taking into account that PC12 neurites show radius variations <10% (Fig. 3), the relative variations of drag force are <1%; consequently, this method ensures a constant force field applied over the sample when neurites are correctly aligned.

Viscoelastic approximation

In the case of slow elongation velocity, to measure the internal friction γ, the response of the molecular motors $T_a e^{-\delta l^2/\nu^2}$ can be approximated to T_a, and the Eq. 7 can be written as

$$\dot{u} + \frac{u}{\tau} + \frac{3\mathcal{T}}{2\gamma L}u^{1/3} = \left(\frac{3}{32}\right)^{1/2}\frac{\omega}{\gamma}, \quad (13)$$

with $\mathcal{T} = T_a - k\delta_\kappa^0$, $u = (\delta l/L)^{3/2}$, and $\tau = 2\gamma/3k$. Equation 13 has no analytical solution; however, it is possible to obtain three approximated solution from the comparison of the initial neurite tension and the applied external force over the neurite curvature, T and ω/C (or, $3\mathrm{T}u^{1/3}/2\gamma L$ and $(3/32)^{1/2}\omega/\gamma$).

The first case, T >> ω/C, leads to a contraction of the neurite given by the global molecular motor activity, where the solution is given by $\delta l(t) = (k\delta_\kappa^0 - T_a)(1 - e^{-\mathrm{kt}/\gamma})/k$, with a final state of the neurite elongation $\delta_\kappa^0 - T_a/k$.

A second case is found when T ~ ω/C, i.e., the tension imposed by the flow compares to the force that molecular motors are able to exert, i.e., $3\mathrm{T}u^{1/3}/2\gamma L - (3/32)^{1/2}\omega/\gamma \sim 0$, with a solution

$$\delta l(t) = \left(\left(\frac{3}{32}\right)^{1/2} - \frac{\mathcal{T}}{\omega L}\right)^{2/3}\left(\frac{L\Theta\omega}{\gamma}\right)^{2/3}\left(1 - e^{-t/\Theta}\right)^{2/3}, \quad (14)$$

with $\Theta^{-1} = \tau^{-1} + \mathrm{T}/2L\gamma$ as the new timescale for the relaxation process, which in the case of early stages of viscous relaxation, $k\delta l \sim 0$ and $t < \Theta$, states that the external force is balanced only by the internal friction of the neurite and its initial tension,

$$\delta l(t) = \left(\left(\frac{3}{32}\right)^{1/2} - \frac{\mathcal{T}}{\omega L}\right)^{2/3}\left(\frac{\omega t}{\gamma}\right)^{2/3}L. \quad (15)$$

Note that most of our experimental data shows ratios $\mathcal{T}/\omega L \lesssim 0.3$.

The last case is obtained when the applied force is larger than the global molecular motors tension $\mathcal{T} << \omega/C$, i.e., the elongation rate is larger than the typical scale velocity, and the molecular motor activity can be ignored. This limit is contained in Eq. 14 at T $\to$ 0; then the solution becomes $\delta l(t) = 2^{-1}\cdot 3^{-1/3}(\omega/k)^{2/3}(1 - e^{-3kt/2\gamma})^{2/3}L$, and for early states of elongation $t < \tau$,

$$\delta l(t) = \left(\frac{3}{32}\right)^{1/3}\left(\frac{\omega t}{\gamma}\right)^{2/3}L. \quad (16)$$

Timescale for relaxation oscillations

To obtain the timescale τ_{relax} for relaxation cycles in Fig. 6, we crudely approximate the molecular motor response by a triangular function of amplitude T_a and width $2v$, then Eq. 7 at the positive rate of elongations region becomes

$$k\delta l + \gamma\dot{\delta l} + T_a - \frac{T_a}{v}\dot{\delta l} = T(\delta l).$$

Considering $T(\delta l) \sim T_a$, $\delta l = \delta l_o + \varepsilon$ and $\delta l_o = \omega^2 L^3/24T_a^2$, we obtain

$$\left(\gamma - \frac{T_a}{v}\right)\dot{\varepsilon} + \left(k + \frac{12T_a^3}{\omega^2 L^3}\right)\varepsilon = -k\delta l_o,$$

with

$$\tau_{relax} = \frac{(\gamma - T_a/v)\omega^2 L^3}{12T_a^3 + k\omega^2 L^3} \approx \frac{L^3}{12T_a^3}\left(\gamma - \frac{T_a}{v}\right)\omega^2.$$

Because τ_{relax} depends on ω^2, τ_{relax} increases a by factor of four when ω is doubled. This is compatible with experimental results presented in Fig. 6 *b*.

Most of the experiments were performed at the Experimentalphysik I, University of Bayreuth. We are very grateful to Francisca Bronfman for valuable help on PC12 cells culture and Jean-Christophe Géminard for many enlightening discussions.

This work was supported by CONICYT-Chile under FONDAP program No. 11980002.

REFERENCES

1. Burton, K., J. H. Park, and D. L. Taylor. 1999. Keratocytes generate traction forces in two phases. *Mol. Biol. Cell.* 10:3745–3769.
2. Oliver, T., M. Dembo, and K. Jacobson. 1999. Separation of propulsive and adhesive traction stresses in locomoting keratocytes. *J. Cell Biol.* 145:589–604.
3. Balaban, N. Q., U. S. Schwarz, …, B. Geiger. 2001. Force and focal adhesion assembly: a close relationship studied using elastic micropatterned substrates. *Nat. Cell Biol.* 3:466–472.
4. Tan, J. L., J. Tien, …, C. S. Chen. 2003. Cells lying on a bed of microneedles: an approach to isolate mechanical force. *Proc. Natl. Acad. Sci. USA.* 100:1484–1489.
5. Dennerll, T. J., P. Lamoureux, …, S. R. Heidemann. 1989. The cytomechanics of axonal elongation and retraction. *J. Cell Biol.* 109:3073–3083.
6. Lamoureux, P., R. E. Buxbaum, and S. R. Heidemann. 1989. Direct evidence that growth cones pull. *Nature.* 340:159–162.
7. Fernández, P., P. A. Pullarkat, and A. Ott. 2006. A master relation defines the nonlinear viscoelasticity of single fibroblasts. *Biophys. J.* 90:3796–3805.
8. Bernal, R., P. A. Pullarkat, and F. Melo. 2007. Mechanical properties of axons. *Phys. Rev. Lett.* 99:018301.
9. Bausch, A. R., W. Möller, and E. Sackmann. 1999. Measurement of local viscoelasticity and forces in living cells by magnetic tweezers. *Biophys. J.* 76:573–579.
10. Coppin, C. M., J. T. Finer, …, R. D. Vale. 1996. Detection of sub-8-nm movements of kinesin by high-resolution optical-trap microscopy. *Proc. Natl. Acad. Sci. USA.* 93:1913–1917.
11. Veigel, C., J. E. Molloy, …, J. Kendrick-Jones. 2003. Load-dependent kinetics of force production by smooth muscle myosin measured with optical tweezers. *Nat. Cell Biol.* 5:980–986.
12. Wu, H. W., T. Kuhn, and V. T. Moy. 1998. Mechanical properties of L929 cells measured by atomic force microscopy: effects of anticytoskeletal drugs and membrane crosslinking. *Scanning.* 20:389–397.
13. Jacobs, J. R., and J. K. Stevens. 1986. Experimental modification of PC12 neurite shape with the microtubule-depolymerizing drug nocodazole: a serial electron microscopic study of neurite shape control. *J. Cell Biol.* 103:907–915.
14. Spector, I., N. R. Shochet, …, A. Groweiss. 1983. Latrunculins: novel marine toxins that disrupt microfilament organization in cultured cells. *Science.* 219:493–495.
15. Lifshitz, E. M., and L. D. Landau. 2000. Fluid Mechanics. Butterworth-Heinemann, MA.
16. Lifshitz, E. M., and L. D. Landau. 2000. Theory of Elasticity. Butterworth-Heinemann, MA.
17. Howard, J. 2001. Mechanics of Motor Proteins and the Cytoskeleton. Sinauer, Sunderland, MA.
18. Teichman, J., and L. Mahadevan. 2003. The viscous catenary. *J. Fluid Mech.* 478:71–80.
19. Coelho Neto, J., U. Agero, …, O. N. Mesquita. 2006. Measuring optical and mechanical properties of a living cell with defocusing microscopy. *Biophys. J.* 91:1108–1115.
20. Bausch, A. R., F. Ziemann, …, E. Sackmann. 1998. Local measurements of viscoelastic parameters of adherent cell surfaces by magnetic bead microrheometry. *Biophys. J.* 75:2038–2049.
21. Dennerll, T. J., H. C. Joshi, …, S. R. Heidemann. 1988. Tension and compression in the cytoskeleton of PC-12 neurites. II: Quantitative measurements. *J. Cell Biol.* 107:665–674.
22. Fujita, H., and S. Ishiwata. 1998. Spontaneous oscillatory contraction without regulatory proteins in actin filament-reconstituted fibers. *Biophys. J.* 75:1439–1445.
23. Salbreux, G., J. F. Joanny, …, P. Pullarkat. 2007. Shape oscillations of non-adhering fibroblast cells. *Phys. Biol.* 4:268–284.
24. Jülicher, F., and J. Prost. 1997. Spontaneous oscillations of collective molecular motors. *Phys. Rev. Lett.* 78:4510–4513.
25. Roux, A., G. Cappello, …, P. Bassereau. 2002. A minimal system allowing tubulation with molecular motors pulling on giant liposomes. *Proc. Natl. Acad. Sci. USA.* 99:5394–5399.
26. Liu, A. P., D. L. Richmond, …, D. A. Fletcher. 2008. Membrane-induced bundling of actin filaments. *Nat. Phys.* 4:789–793.